NANO LETTERS

2001
Vol. 1, No. 8
443−447

Phase Transformation, Coalescence, and Twinning of Monodisperse FePt Nanocrystals

Z. R. Dai,[†] Shouheng Sun,[‡] and Z. L. Wang*,[†]

School of Materials Science and Engineering, Georgia Institute of Technology, Atlanta, Georgia 30332-0245, and IBM T. J. Watson Research Center, Yorktown Heights, New York 10598

Received June 7, 2001; *Revised Manuscript Received June 25, 2001*

ABSTRACT

The phase transformation, coalescence, and twin structure of thermally annealed 6 nm FePt nanocrystals under high vacuum on an amorphous carbon surface have been investigated. A1-FePt phase to $L1_0$–FePt phase transformation occurs at 530 °C. The multilayered nanocrystal assemblies coalesce to form larger grains at 600 °C. These coalesced nanocrystals do not form a single grained structure; instead, twinning becomes a characteristic structure feature. The surface of the coalescent grains consists of {111} and (001) facets.

The iron−platinum (Fe−Pt) alloys have been investigated for several decades because of their important applications in permanent magnetism.[1−7] Depending on the Fe to Pt elemental ratio, these alloys can display chemically disordered face centered cubic (fcc) phase (A1, $Fm\bar{3}m$) or chemically ordered phases, such as ($L1_2$, $Pm\bar{3}m$) for Fe_3Pt, face centered tetragonal (fct) phase ($L1_0$, *P*4/*mmm*) for FePt and ($L1_2$, $Pm\bar{3}m$) for Pt_3Fe.[8,9] These structure variations have dramatic effects on the magnetic properties of the alloys. For example, the Fe_3Pt material is paramagnetic,[10] the Pt_3Fe is antiferromagnetic, while the $L1_0$ structured FePt has a large uniaxial magnetocrystalline anisotropy ($K_u \cong 7 \times 10^6$ J/m^3)[13,14] and shows strong ferromagnetic properties.[12] Various experimental results have revealed that the $L1_0$ type structure can be formed in Fe_xPt_{1-x}, with x ranging from 0.35 to 0.60.[15] The iron-rich $L1_0$-FePt alloy-based nanoparticle materials have shown excellent hard magnetic properties[5,16,17] and are expected to be used for a new generation of ultrahigh-density magnetic recording media.[17−19]

To fully understand the magnetics of these FePt-based nanomaterials, it is essential to synthesize monodisperse FePt particles with controlled size and composition and study the structure transformation within each particle after various thermal treatments. It will be also important to know the aggregation behaviors of these annealed nanoparticles. The synthesis has been attempted by various vacuum deposition techniques.[20−23] However, random nucleation in the process generally results in broad distributions of particles sizes, which complicates the observations on particle structure transformation, and further on particle magnetics. Recently, monodisperse FePt nanocrystals with good control on particle size and composition were produced by a solution-phase chemical procedure.[17] These monodisperse FePt nanocrystals become ideal candidates for microscopic study on thermal annealing induced structure transformation. Previous thermal annealing experiments have shown that, for stoichiometrical bulk FePt alloy, the A1 to $L1_0$ transformation temperature is 1300 °C,[15] while for nanoscale FePt particles, this temperature is lowered to within 500−700 °C, depending on FePt stoichiometry and particle sizes.[17,24]

We report detailed microscopic studies on phase transformation, coalescence, and twin structure formation of thermally annealed 6 nm FePt nanocrystals under high vacuum on an amorphous carbon surface. Our transmission electron microscopy (TEM) studies show that A1 to $L1_0$ phase transformation occurs at 530 °C. The multilayered nanocrystal assemblies coalesce to form larger grains at 600 °C. We notice that the coalescent temperature of the nanocrystal monolayer assembly depends on the substrate used. On SiO_2 substrate, the FePt nanocrystal monolayer can stand up to 700 °C without any obvious aggregation. The coalesced nanocrystals show dominant {111} twin defect inside, while their surface and coalescent grain boundary consist of both {111} and (001) facets.

The monodisperse FePt nanocrystals are synthesized by reduction of platinum acetylacetonate ($Pt(CH_3COCHCOCH_3)_2$) and decomposition of iron pentacarbonyl ($Fe(CO)_5$) in the presence of oleic acid and oleylamine stabilizers.[17] The size and composition of the FePt nanoparticles can be readily

* Corresponding author e-mail: zhong.wang@mse.gatech.edu
[†] Georgia Institute of Technology.
[‡] IBM T. J. Watson Research Center. E-mail: ssun@us.ibm.com

10.1021/nl0100421 CCC: $20.00
Published on Web 07/12/2001

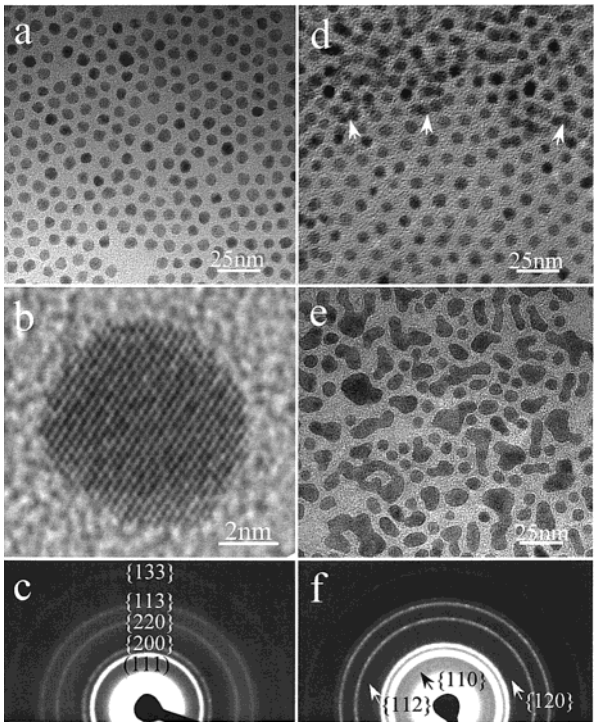

Figure 1. TEM image of the as-synthesized $Fe_{52}Pt_{48}$ nanocrystals (a) and the corresponding select area electron diffraction pattern (c). (b) HRTEM images of the as-synthesized individual $Fe_{52}Pt_{48}$ nanocrystals. TEM images of the $Fe_{52}Pt_{48}$ nanocrystals after annealing at 530 °C for 1 h (d) and at 600 °C for 1 h (e). Select area electron diffraction patterns of the $Fe_{52}Pt_{48}$ nanocrystals recorded in-situ at 530 °C for 1 h.

controlled. Their composition is adjusted by controlling the molar ratio of iron carbonyl to the platinum salt. In the present study, the 6 nm FePt nanocrystals are synthesized by first growing 3-nm monodisperse FePt seed crystals and then adding more reagents to enlarge the seed crystals to the desired size under a 2:1 molar ratio of iron carbonyl to the platinum salt. These nanocrystals are isolated and purified by centrifugation after the addition of a flocculent (for example, ethanol) and can be redispersed in nonpolar solvents in a variety of concentrations.

TEM samples were prepared by depositing a drop of dilute FePt dispersion onto a carbon-coated copper grid. The phase transformation was investigated by using a heating specimen holder under a Hitachi HF-2000FE field emission transmission electron microscope operating at 200 kV. The heating speeds were controlled to be ~10 °C/min before 400 °C and ~5 °C/min after 400 °C. Isothermal processing was carried out at 400 °C, 450 °C, 500 °C, 530 °C, 550 °C and 600 °C, respectively, for 30−60 min. The chemical ordering, coalescence, and twin structure were studied by using a JEOL-4000EX high-resolution transmission electron microscope (spherical aberration coefficient Cs = 1.0 mm) at 400 kV.

Shown in Figure 1(a) is a low magnification TEM image of the as-synthesized monodisperse FePt nanocrystals. The size of FePt nanocrystals is about 6 nm in diameter. High resolution transmission electron microscopy (HRTEM) observation of an individual nanocrystal (Figure 1b) indicates very good crystallinity and a dominant truncated octahedral shape. The truncated octahedral is enclosed by the {100} and {111} crystal facets of the fcc structure, indicating that the as-synthesized FePt nanocrystals have a chemically disordered fcc (A1) phase of which lattice parameter is a = 0.376 nm. The fcc structure feature of the as-synthesized FePt nanocrystals is also shown in their electron diffraction pattern. Figure 1c is such a pattern from the selected area of diffraction of the nanocrystal assembly. The composition of the nanocrystals is determined to be very close to $Fe_{52}Pt_{48}$ by energy-dispersive X-ray spectroscopy (EDS).

To study the phase transformation from the chemically disordered A1-FePt phase to the chemically ordered ferromagnetic $L1_0$-FePt phase, in situ thermal annealing is applied to the as-synthesized FePt nanocrystal assembly. At temperatures below 450 °C, no obvious assembly or structure change is observed. At temperatures beyond 450 °C, multilayered nanocrystal assemblies start to decay gradually. Further annealing at 530 °C transforms the chemically disordered A1 phase to chemically ordered $L1_0$ phase. The TEM image (Figure 1d) shows the morphology of FePt nanocrystals isothermally treated at 530 °C for 1 h. It shows that most of the hexagonally packed monolayer nanocrystal assemblies are almost intact, while regular arrayed multilayer assemblies are deteriorated by this thermal treatment. The corresponding electron diffraction pattern is shown in Figure 1f. Comparing the diffraction patterns shown in Figure 1f with those in Figure 1c, different reflection rings, such as {110}, {120}, {112}, etc., appear, indicating occurrence of the phase transformation from chemically disordered A1 fcc phase to chemically ordered $L1_0$ fct phase. Continually heating the specimen at higher temperature results in the coalescing of these nanocrystals. Figure 1e shows a TEM image taken from the specimen undergoing an isothermal treatment at 600 °C for 1 h, after which most of nanocrystals, especially in the multilayer region, coalesce with only some dots in the monolayer region staying intact. Figure 2a is a HRTEM image of one of the intact FePt nanocrystals. Comparing with the image shown in Figure 1b, an intensity modulation of image spots can be identified, as marked by arrowheads in the Figure 2a, indicating the formation of the chemically ordered $L1_0$−FePt structure. To illustrate the detailed atomic arrangement within a single nanocrystal, an enlarged HRTEM image is shown in Figure 2b. Fast Fourier transformation (FFT) of such atomic arrangement reveals distorted 2-fold symmetry, as shown in Figure 2c. This diffraction pattern matches well with that generated from theoretical simulation based on dynamic diffraction theory for the $L1_0$-FePt structure (Figure 2d) with the [110] beam and lattice parameters a = 0.3861 nm and c= 0.3788 nm. HRTEM image of the atomic arrangement obtained from the simulation (Figure 2e) is identical to the image shown in Figure 2b, confirming the intensity modulation occurring along c-axis of the $L1_0$-FePt Phase, along which Fe and Pt atoms stack alternately, i.e., the intensity change of image spots along the c-axis is due to chemically ordering (composition modulation) in the $L1_0$-FePt structure.

The structure of the coalesced FePt nanocrystals has also been studied. Figures 3a and 3b are two HRTEM images of

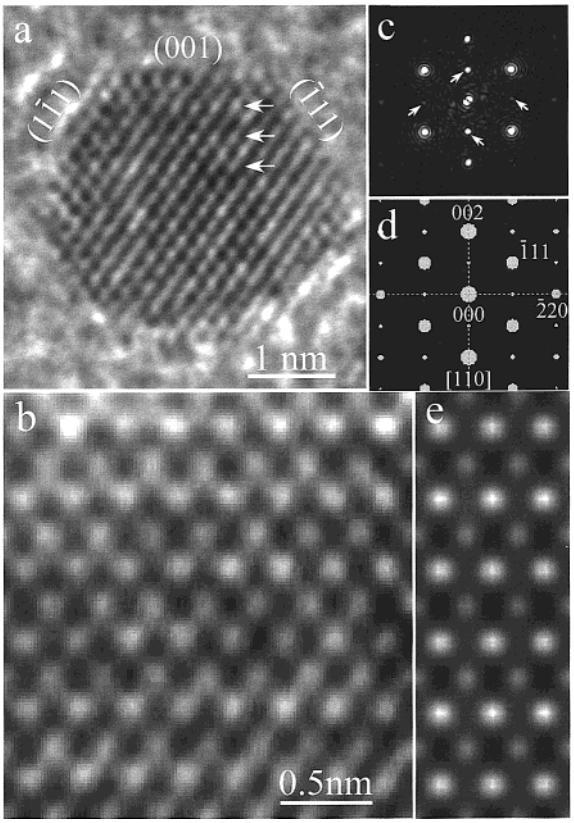

Figure 2. (a) HRTEM image of an individual $Fe_{52}Pt_{48}$ nanocrystal after annealing at 530 °C for 1 h. An enlarged HRTEM image of the chemically ordered $L1_0$-FePt structure (b) and a Fourier transform of the corresponding HRTEM image (c). (d) Simulated electron diffraction pattern, and (e) the corresponding simulated HRTEM image demonstrated under the conditions: 400 kV, Cs = 1.0 mm, thickness = 8 nm, defocus = −74 nm and beam divergence = 0.15 mrad.

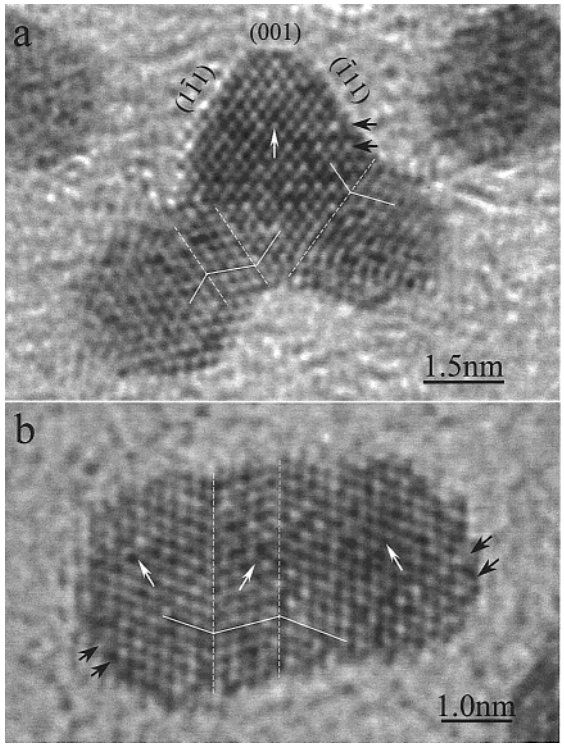

Figure 3. (a) and (b) HRTEM images of coalescent $Fe_{52}Pt_{48}$ grains after annealing at 600 °C for 1 h.

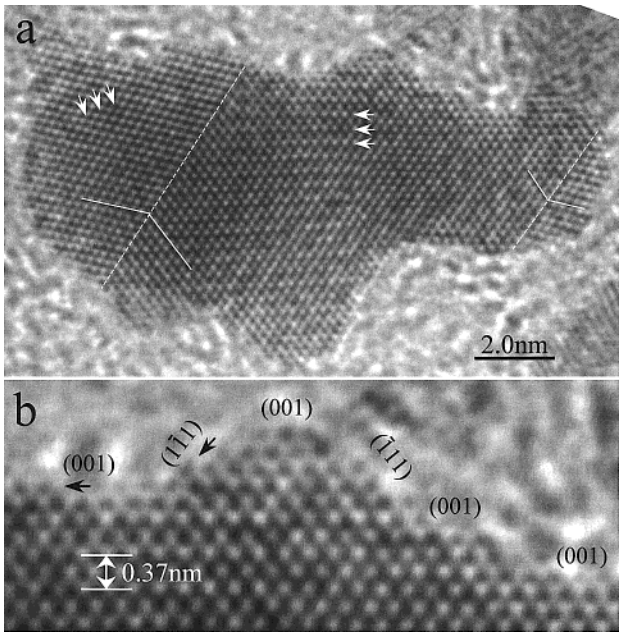

Figure 4. (a) HRTEM image of a large coalescent $Fe_{52}Pt_{48}$ grain after annealing at 600 °C for 1 h. (b) HRTEM image showing surface structure of a coalescent $Fe_{52}Pt_{48}$ grain.

the typical coalescent large FePt grains. The grain shown in Figure 3a consists of three individual FePt nanocrystals and, in Figure 3b, is from two nanocrystals. Twinning is a characteristic feature of the microstructure of the coalescent grains. The dashed lines marked in Figures 3a and 3b represent twin boundaries in the coalescent FePt grains, which usually form a coherent or semi-coherent interface between coalesced FePt nanocrystals. The composition modulation in the $L1_0$-FePt structure is indicated by black arrowheads in Figure 3a,b . The white arrowheads indicate the direction of magnetic easy axis, i.e., the *c*-axis direction of $L1_0$-FePt. The HRTEM image shown in Figure 4a is a large coalescent FePt grain in which original FePt nanocrystals coherently coalesce together to form a chemically ordered $L1_0$-FePt phase, where white arrowheads indicate the composition modulation. Two twin boundaries are identified in the grain, as marked by dashed lines. The interfaces between composed FePt nanocrystals, however, cannot be distinguished. Another structural feature of the annealed FePt nanocrystals is that the surface of the $L1_0$-FePt nanocrystal (Figure 2a) and the grain (Figure 3a) consists of {111} and (001) crystal facets, which have lower surface energy for metals. Figure 4b shows an enlarged HRTEM image of the $L1_0$-FePt grain surface where the atomic stage can be identified on both {111} and (001) facets, as indicated by black arrowheads.

The detailed atomic arrangement of the twin structure in $L1_0$-FePt grain is investigated by HRTEM, as shown in Figure 5a. The electron beam used for imaging is parallel to the [110] crystal direction of the $L1_0$-FePt structure. Figure 5c is an FFT of the corresponding image of Figure 5a. It reveals the main reflections that display a typical diffraction

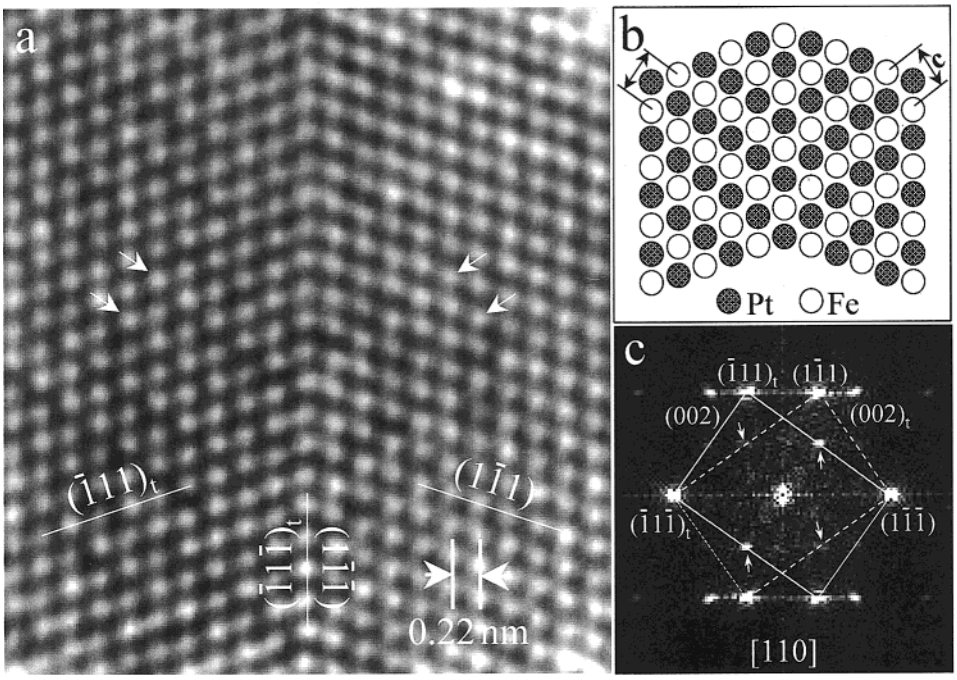

Figure 5. (a) HRTEM image showing a twin boundary in the ordered $L1_0$ structure. (b) The projected twin structure model. (c) Fourier transform of the corresponding image in (a).

feature of the (111) twin in the fct lattice structure. The reflections connected by solid and dashed lines are from twin and matrix, respectively. Some extra weak reflections, as indicated by white arrowheads in Figure 5c, originate from chemical ordering over the $L1_0$-FePt structure. The corresponding composition modulation can be clearly identified from the HRTEM image (Figure 5a) marked by white arrowheads. A possible atom model of the twin structure is given in Figure 5b, where the open circles represent Fe atoms and the full circles are Pt atoms. Therefore, the twin plane is parallel to $(1\bar{1}\bar{1})$ or $(\bar{1}1\bar{1})_t$, where the subscript "t" denotes twin reflection to distinguish from those of the matrix, and the *c*-axes of the twin and matrix are on the same plane and form a mirror symmetry relative to the $(1\bar{1}\bar{1})$ or $(\bar{1}1\bar{1})_t$ twin plane. Since the magnetic easy axis is parallel to the *c*-axis of the $L1_0$-FePt crystal structure, the magnetizing directions for twin and matrix should display the mirror symmetry relative to the twin plane.

The twin structure presented above may be closely related to the size of the coalesced grains. Crystal defects, which have been observed in the bulk and thin $L1_0$-FePt film, are mainly plane defects, such as twin and antiphase domain boundary.[25−30] It has been suggested that these defects are associated with magnetic hardness of the $L1_0$-FePt.[28−30] In the bulk $L1_0$-FePt, the twin structure has been determined to be the {110} type, i.e., the twinning plane is {110}.[25,28] The {111} type twin was observed in FePt film.[29,30]

We have presented a detailed high-resolution microscopic study on phase transformation, coalescence, and twin microstructure of thermally annealed monodisperse 6 nm $Ft_{52}Pt_{48}$ nanocrystals. The crystal transformation temperature is consistent with previous observations,[17] but the presence of vacuum induces the easier coalescence of the nanocrystals on carbon surface than on SiO_2 surface. These coalesced nanocrystals do not form a single grained structure; instead, twinning becomes a characteristic structure feature. The surface of the coalescent grains consists of {111} and (001) facets,[31] which will certainly decide the shape of the new grains. Such detailed analyses yield basic structural information on the nanocrystal behaviors under high vacuum annealing conditions, and will be useful for future fabrication of FePt nanoparticle-based high-density magnetic recording media.

References

(1) Graf, L.; Kussmann, A. *Z. Phys.* **1935**, *36*, 544.
(2) Lipson, H.; Shoenberg, D.; Stupart, G. V. *J. Inst. Met.* **1941**, *67*, 333.
(3) Franklin, A. D.; Berkowitz, A. E.; Klokholm, E. *Phys. Rev.* **1954**, *94*, 1423.
(4) Darling, S. *Platinum Met. Rev.* **1963**, *7*, 96.
(5) Watanabe, K.; Masumoto, H. *Trans. Jpn. Inst. Met.* **1983**, *9*, 627.
(6) Tanaka, Y.; Kimura, N.; Hono, K.; Yasuda, K.; Sakurai, T. *J. Magn. Magn. Mater.* **1997**, *170*, 289.
(7) Watanabe, M.; Masumoto, T.; Ping, D. H.; Hono, K. *Appl. Phys. Lett.* **2000**, *76*, 3971.
(8) Cabri, L. J.; Owens, D. R.; Laflamme, J. H. G. *Can. Mineral.* **1973**, *12*, 21.
(9) Cabri, L. J.; Feather, C. E. *Can. Mineral.* **1975**, *13*, 117.
(10) Liu. J. P.; Luo, C. P.; Liu, Y.; Sellmyer, D. J. *Appl. Phys. Lett.* **1998**, *72*, 483.
(11) Crangle, J. *J. Phys. Radium* **1959**, *20*, 435.
(12) Westbrook, J. H. *Intermetallic Compounds*, John Wiley & Sons: New York, 1967; p 541.
(13) Ivanov, O. A.; Solina, L. V.; Demshina, V. A.; Magat, L. M. *Phys. Met. Metallogr.* **1973**, *35*, 81.
(14) Inomata, K.; Sawa, T.; Hashimoto, S. *J. Appl. Phys.* **1988**, *64*, 2537.
(15) Hansen, M. *Constitution of Binary Alloys*, McGraw-Hill: New York, 1958; p 689.
(16) Watanabe, K.; Masumoto, H. *Trans. Jpn. Inst. Met.* **1985**, *26*, 362.
(17) Sun, S.; Murray, C. B.; Weller, D.; Folks, L.; Moser, A. *Science* **2000**, *287*, 1989.
(18) Weller, D.; Moser, A. *IEEE Trans. Magn.* **1999**, *35*, 4423.

(19) Christodoulides, J. A.; Huang, Y.; Zhang, Y.; Hadjipanayis, G. C.; Panagiotopoulos, I.; Niarchos, D. *J. Appl. Phys.* **2000**, *87*, 6938.
(20) Coffey, K. P.; Parker, M. A.; Howard, J. K. *IEEE Trans. Magn.* **1995**, *31*, 2737.
(21) Liu, J. P.; Liu, Y.; Luo, C. P.; Shan, Z. S.; Sellmyer, D. J. *J. Appl. Phys.* **1997**, *81*, 5644.
(22) Li, N.; Lairson, B. M. *IEEE Trans. Magn.* **1999**, *35*, 1077.
(23) Risrau, R. A.; Barmak, K.; Lewis, L. H.; Coffey, K. R.; Howard, J. K. *J. Appl. Phys.* **1999**, *86*, 4527.
(24) Bae, S. Y.; Shin, K. H.; Jeong, J. Y.; Kim, J. G. *J. Appl. Phys.* **2000**, *87*, 6953.
(25) Kandaurova, G. S.; Onoprienko, L. G.; Sokolovskaya, N. I. *Phys. Stat. Sol. (a)* **1982**, *73*, 351.
(26) Gau, J. S.; Mishra, R. K.; Thomas, G. *IEEE Trans. Magn.* **1983**, *MAG-19*, 2256.
(27) Kandaurova, G. S.; Onoprienko, L. G.; Vlasova, N. I. *Phys. Met. Metallogr.* **1987**, *64*, 16.
(28) Zhang, B.; Soffa, W. A. *Phys. Stat. Sol. (a)* **1992**, *131*, 707.
(29) Hong, M. H.; Hono K.; Watanabe, M. *J. Appl. Phys.* **1998**, *84*, 4403.
(30) Bian, B.; Laughlin, D. E.; Sato, K.; Hirotsu, Y. *J. Appl. Phys.* **2000**, *87*, 6962.
(31) Research was supported by the U.S. National Science Foundation (DMR-9733160).

NL0100421